Energy exchange during electron emission from carbon nanotubes: Considerations on tip cooling effect and destruction of the emitter

M. Dionne,* S. Coulombe, and J.-L. Meunier
Department of Chemical Engineering, McGill University, 3610 University Street, Montreal, Quebec, Canada H3A 2B2
(Received 1 May 2009; revised manuscript received 19 June 2009; published 26 August 2009)

Murphy and Good general theory for electron emission from metal surfaces was used to predict the field emission capabilities of ideal arrays of vertically aligned carbon nanotubes (VACNT). The Nottingham effect was taken into account in order to explain the experimental observation of a localized cooling of the VACNT tips caused by field emission and the destruction of the very short emitters at strong currents. Our model allowed to match the current, voltage, and observed breaking points of individual VACNT reported in two separate experimental studies.

DOI: 10.1103/PhysRevB.80.085429 PACS number(s): 73.63.Fg

I. INTRODUCTION

The electric current-induced destruction of carbon nanotube (CNT) field emitters was studied by Wei *et al.*[1] using a simplified model for the heat exchange associated with electron emission. Their model assumed that each electron takes away an energy $\Delta\varepsilon=\frac{3}{2}k_BT_s$ upon leaving the surface, where T_s is the surface temperature. The consequence of using this electron emission cooling mechanism was a localized cooling of the CNT tip during field emission, partially compensating for the Joule heating. As a result, the predicted longitudinal temperature profile showed a maximum temperature value occurring somewhere along the CNT body. Once this peak temperature reached the critical temperature initiating etching of carbon by trace amounts of oxygen,[2] a breaking of the CNT was predicted at this location. Therefore, it was deduced that a section of the emitter would be taken away. When this electron emission cooling effect was not included, the hottest point was located at the CNT tip and the predicted tip-based destruction mechanism was referred to as field-assisted evaporation.[3] High temperatures are usually assumed to be responsible for the destruction of CNTs during field emission. However the use of simpler models while simultaneously assuming high surface temperatures T_s and strong surface electric fields E_s may lead to important errors. Furthermore, the approach taken by Wei *et al.* also overlooks some additional energy transport mechanisms.

Electron emission from metal surfaces is driven by high T_s and/or E_s. The electron emission is usually categorized into three regimes, known respectively as field emission (low T_s, high E_s), thermionic emission (high T_s, low E_s), and thermo-field (T-F) emission (both high T_s and E_s). A general theoretical description of electron emission was provided by Murphy and Good (M-G) (Ref. 4) who introduced a complex integral expression for the electron current density $J_{\text{M-G}}$ that can be evaluated numerically. More recent studies[5,6] have provided analytical expressions for $J_{\text{M-G}}$; numerical methods based on Ref. 4 will however be used in this work. A consequence of the complexity in evaluating the general expression resulted in the much simpler Fowler-Nordheim[7] and Richardson-Dushman[8] analytical equations that are widely used respectively for field ($J_{\text{F-N}}$) and thermionic ($J_{\text{R-D}}$) emission. Since these equations originate from simplifications of the M-G theory, they can be expected to digress from the actual $J_{\text{M-G}}$ prediction, especially as the T-F regime is approached. This fact has been known for some time (see Ref. 9) but the scale of the discrepancies with the actual T-F emission has not always been clear. Our previous work[10] demonstrated that $J_{\text{R-D}}$ always underestimates $J_{\text{M-G}}$ significantly and thus, we concluded that the use of the M-G equation is necessary for $E_s=10^{7-10}$ V/m, $T_s=1000-5000$ K, and for all values of the work function, ϕ_0. In a recent study[11] we compared $J_{\text{F-N}}$ to $J_{\text{M-G}}$ based on a discussion from Paulini *et al.*[12] where it was pointed out that the F-N equation underestimates $J_{\text{M-G}}$ by a factor 10^{2-6} at 1000 K and above. Our calculations indicated that for the particular value $\phi_0=4.5$ eV used for CNTs, this factor is nearly constant and close to 10^2. It then appeared necessary to use $J_{\text{M-G}}$ in all circumstances. M-G theory also provides a better description of the energy loss or gain experienced by the crystalline lattice of a given material during the electron emission process. This phenomenon, known as the Nottingham effect (see Ref. 12), can either heat or cool the surface depending on whether the replacing electron coming from the external circuit has an energy greater or lower than that of the emitted electron. Richardson theory accounts for cooling only, in an inaccurate way, especially as E_s increases.

In this study, we first review important concepts of M-G theory and discuss the origin of the Nottingham effect as a potential cooling or heating mechanism for a surface. As a second step, we study the CNT self-heating experiment performed by Wei *et al.*[1] to estimate the CNT thermal conductivity k_{CNT}, room-temperature resistivity ρ_0, and thermal contact resistance λ_1 between the CNT and its support (a tungsten microtip). Thirdly, the Nottingham effect is studied separately to predict its potential role as a heating or cooling mechanism during field emission. The achievable surface-averaged current density J_{eq} (A/m^2) is then predicted using M-G theory for vertically aligned carbon nanotube (VACNT) arrays of different lengths h and radii r, assuming a constant spacing Δx between ideal emitters put in good electrical and thermal contact with a copper substrate. The combined contributions of Joule heating and Nottingham cooling/heating on the longitudinal temperature profile within the emitter are discussed. A particular attention is given to the apparently problematic cases characterized by

smaller CNT aspect ratios ($h/r \leq 20$) for which the Wei *et al.*[1] model could not provide a correct prediction for the location of the CNT breaking point.

II. THEORY

We first discuss the M-G theory and predicted values of the electron emission current density, $J_{\text{M-G}}$, and Nottingham energy exchange ε_{Not} representing the energy gain (or loss) experienced by the surface. The predictions of these models are studied independently before inclusion in our set of governing equations describing the energy transport in a CNT maintained under conditions providing strong electron emission.

For a complete description of the electron emission process, we refer the reader to the original work of Murphy and Good,[4] the study of Paulini *et al.*,[12] and our previous work.[10,11] $J_{\text{M-G}}$ is given by Eq. (1). A number of studies have been dedicated to the Nottingham effect over the years and for additional information the reader is encouraged to consult[13] as well as the references therein.

$$J_{M-G} = e\int_{-W_a}^{\infty} D(E_s,W)N(W,T_s,\phi_0)dW \tag{1}$$

where $-W_a$ is the effective constant potential for the electron inside the emitter, W is the energy of an incident electron on the potential barrier in the direction perpendicular to the surface, $D(E_s,W)$ is the probability for the electron of energy W to penetrate the barrier, and $N(W,T_s,\phi_0)dW$ is the number electrons within the dW energy interval. Once $J_{\text{M-G}}$ is known, Fermi-Dirac statistics can be used to provide ε_{Not} as indicated by Eqs. (2)–(4) where $E=p^2/2m_e+V$ is the total energy of an electron, with p and V being respectively the momentum and potential energy of the electron. In these calculations we used the vacuum level as the zero energy for the variables W and E

$$\varepsilon_{\text{Not}} = \frac{e}{J_{\text{M-G}}}\int_{-\infty}^{\infty} EP_E(E,E_s,T_s,\phi_0)dE + \phi_0 \tag{2}$$

$$P_E(E,E_s,T_s,\phi_0) = \int_{-\infty}^{E} N_E(E,T_s,\phi_0)D(E_s,W)dW \tag{3}$$

$$N_E(E,T_s,\phi_0) = -\frac{4\pi m_e}{h^3}\frac{1}{1+\exp\left(\dfrac{E+\phi_0}{k_BT_s}\right)}. \tag{4}$$

In Eq. (2) the second term (ϕ_0) represents the energy of the replacing electron (i.e., the Fermi energy ε_{F}). It has been predicted in Ref. 14 that the energy of the replacing electrons will be shifted from the value ε_{F} by a few tens of meV but only for high temperatures (>2500 K) and very strong electric fields ($>10^{10}$ V/m) which are beyond our intervals of interest. As a consequence the value of ε_{F} is a valid choice for all results reported in this study. P_E is the probability for a number density N_E of electrons of energy E to penetrate the potential barrier at the metal-vacuum interface. At low temperature and as the applied electric field becomes strong enough, electrons originating from energy states located under the Fermi level will tunnel through the surface potential barrier. Since the replacing electron supplied from the electrical circuit carries an energy equal to the metal work function, the overall energy exchange is positive, thus leading to a heating of the surface due to electron tunneling. Conversely, in the case of high surface temperatures, the number of electrons having energies larger than ε_{F} is significant enough to supply most of the emission current, and the replacing electrons must absorb energy from the lattice in order to occupy the energy states emptied by the emitted electrons. The electron emission process thus becomes a cooling mechanism.

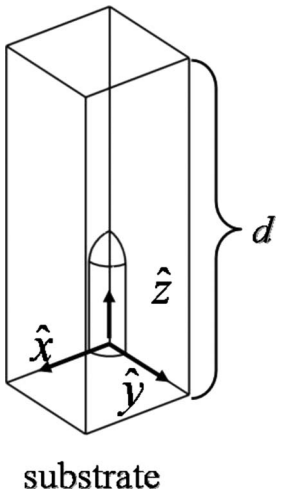

FIG. 1. Schematic representation of a single VACNT on the substrate.

III. DESCRIPTION OF THE ELECTRICAL/ THERMAL MODEL

Figure 1 shows a VACNT standing at the origin of a 3D Cartesian grid on the metal substrate. When a potential difference ΔV is applied between this surface and a flat anode located at a distance d from the metal substrate, the magnitude of the electric field $|\vec{E}|$ around the VACNT is greater than the value obtained from the one-dimensional (1D) solution ($E_0=\Delta V/d$) one finds between two infinite flat electrodes. To quantify this effect, the field enhancement factor $\beta=|\vec{E}|/E_0$ is defined. For a VACNT structure, the Laplace equation can be solved above the cathode surface to provide the three-dimensional (3D) distribution of β. To simulate the presence of other elements in the case of a VACNT array, symmetry conditions can be assumed at the limits of the computational domain along the $\hat{x}$ and $\hat{y}$ axes. It has been reported[15] that $\beta=1.2(2.15+(h/r)_{\text{CNT}})^{0.9}$ on the tip of an isolated VACNT, where $(h/r)_{\text{CNT}}$ is the ratio between the height (h) and radius (r) of the CNT (i.e., the aspect ratio). It is also known[16] that when two identical VACNTs stand close to each other within a distance Δx similar to h, the value of β on the surface decreases. This phenomenon results from screening effects and causes the value of the equivalent

surface-averaged current density J_{eq} for the array to decrease when the VACNTs are brought closer to each other. When $\Delta x \gg h$, the lower surface density of emitters lowers J_{eq}. As a consequence, an optimal spacing $\Delta x_{optimal}=(1 \text{ to } 2)h$ is found. This was elucidated through the study of three different theoretical arrays and further analysis of experimental data for an isolated VACNT (Refs. 1 and 17) while assuming $\Delta x=2h$.

In order to calculate the emitter temperature, the current and heat conservation equations were solved within the CNT using calculated electrical and thermal properties[18] and experimental data from Refs. 1 and 17. We used constant CNT thermal conductivity values and the following temperature dependent expression for the electrical resistivity, where ρ_0 is the room-temperature value[18]

$$\rho(T) = \rho_0(1 - 8.5 \times 10^{-4}T + 9.8 \times 10^{-6}T^{3/2}). \quad (5)$$

Electron emission was allowed over the entire CNT surface. However, β decreases rapidly with increasing distances from the CNT tips. This reduces the effective emitting surface to the top portion of the CNT caps. As indicated previously, symmetry conditions were used at the limits of the computational domain along the $\hat{x}$ and $\hat{y}$ axes. We assumed $V=0$ at the lower $\hat{z}$ boundary while the distribution of $|\vec{E}|$ on the cathode surface was used to dictate a current density boundary condition with Eq. (1). To that end, we used COMSOL™ "Electrostatics" model to calculate $|\vec{E}|$ in the inter-electrode volume and the "Conductive media dc" model inside the electrode. Due to the large aspect ratio of the CNTs considered, we used an axisymmetric two-dimensional (2D) model for the heat transfer during a self-heating experiment assuming a thermal contact resistance (or a constant temperature) at the contact points of the CNT with a tungsten microtip and a counter-electrode. The electrical and thermal conductivity values we deduced from these calculations were then used in the heat balance of our 3-D field emission model. We used Stefan-Boltzmann radiative cooling from the side walls of the tubes and additional energy exchanges at the tip due to the Nottingham effect. For this matter, a heat flux source term $|\vec{q}|=J_{M\text{-}G}\cdot\varepsilon_{Not}$ was used on the emitting surface, with ε_{Not} calculated self-consistently with the surface electric field. One can expect a heating effect to occur at low emitter temperature until the increasing number of electrons emitted from energy states higher than ε_F allows the Nottingham effect to become a cooling effect (i.e., at high emitter temperature). This transition from heating to cooling is characterized by a critical temperature thereafter named the inversion temperature T_{inv}. In cold emitters, T_{inv} is typically much higher than 300 K for all surface electric fields generating significant electron emission. However when no external heat source is used to impose a high temperature, the actual value of T_s with respect to T_{inv} depends on the intensity of the local Joule heating, which in turn depends on the effective value of E_s. In the case of very small electron emission currents, the negligible contribution of Joule heating (proportional to $|\vec{J}|^2$) would lead to a Nottingham effect inducing an interfacial heat source proportional to $|\vec{J}|$ that can be dissipated by heat conduction along the CNT.

IV. RESULTS AND DISCUSSION

First, a CNT self-heating experiment described in Ref. 1 is modeled to evaluate the thermal conductivity, electrical conductivity and thermal contact resistance from their experimental results. The $J_{M\text{-}G}$ and ε_{Not} data are then studied independently to formulate a qualitative prediction for the contribution of the Nottingham effect during field emission when both E_s and T_s are high. We then present the surface-averaged current density $J_{eq}(E_0)$ curves for theoretical VACNT arrays of interest in order to evaluate ideal theoretical performances and compare them to nonideal scenarios. The corresponding ε_{Not} data is then extracted to investigate the evolution of the Nottingham effect between the two possible regimes (cooling or heating). Finally, case studies are performed for the individual VACNT described in Ref. 1 to demonstrate how our model can be used to successfully predict the observed locations for the breaking point. The accuracy of our model is demonstrated by comparing the predictions with available experimental values. Because of the extensive number of variables discussed in the following sections, we refer the reader to Table I for a reminder of the most important definitions. As Table I indicates, many parameters are not calculated in the 1D model of Wei *et al.*[1] Only the heat equation is solved for a given current and the boundary conditions are changed for the CNT self-heating experiment and field emission measurements. We, on the other hand, used a separate 2D axisymmetric model in Sec. A for the study of the CNT self-heating experiment and a 3D model for field emission.

A. CNT self-heating calculations

In order to understand our choice of CNT properties, the reader must consider the supporting information given by Wei *et al.*[1] in the description of their experiment. These authors mounted a single 1080 nm long, multi-walled carbon nanotube (MWCNT) having a diameter of 14 nm on a tungsten microtip and contacted its opposite end to a counter-electrode thus creating a small resistive circuit. A dc voltage ramp was applied leading to the CNT breaking by resistive Joule heating at a distance of 470 nm from the junction with the tungsten microtip (see Fig. 2). This event occurred for an applied voltage $\Delta\psi$ of 2.38 V and a current I of 81 μA. These experimental values hereby become target values our 2D model must match in order to provide valid temperature profiles. In Ref. 1, the surviving fragment was further used as a field emitter. This last geometry will be used in the present study as Case 1, which is referred to in Sec. D.

The authors of Ref. 1 developed a simple radially lumped one-dimensional model for the calculation of the temperature (T) distribution along the length of the current carrying CNT. They considered energy generation in the volume by resistive Joule heating and Stefan-Boltzmann radiation boundary conditions at the CNT outer surface using a surface emissivity of one. The additional energy exchange term at the CNT tip associated with electron emission was accounted for using a simplified model assuming that each emitted electron carries away its thermal energy, i.e., $\Delta\varepsilon=\frac{3}{2}k_BT_S$. The CNT thermal conductivity and thermal contact resistance at the

TABLE I. Comparative list of parameters involved in Ref. 1 and in our models.

Variable	Definition	In Ref. 1	In our models
ε	Cooling/heating associated with electron emission	Cooling, $\Delta\varepsilon=\frac{3}{2}k_BT_s$	Replaced by the model for Nottingham effect (3D)
T_s	Surface temperature	Calculated (1D)	Calculated (3D)
E_s	Surface electric field	Not used	Calculated (3D)
$J_{\text{M-G}}$	Emitted electron current density	Not used	Calculated (3D)
ϕ_0	Emitter work function	Not used	Calculated (3D)
I_{exp}	Measured electron emission current	Measured	Target value for I_{th}
I_{th}	Calculated electron emission current	I_{exp} is used directly (1D)	Calculated (3D)
ΔV_{exp}	Applied voltage (field emission)	Measured but not used	Target value for ΔV_{th}
ΔV_{th}	Calculated applied voltage associated with I_{th}	Measured but not used in the calculations	Calculated (3D)
k_{CNT}	CNT thermal conductivity	100 W/(m.K)	2D: adjusted 3D: deduced from 2D
ρ_0	CNT electrical resistivity at 300 K	Averaged measurement	Adjusted (2D and 3D)
d	Interelectrode gap (field emission)	Measured but not used	Used in the 3D model
β	Electric field enhancement factor	Not used or calculated	Calculated (3D)
ψ	Potential (self-heating experiment)	Not calculated	Calculated (2D)
I	Current (self-heating experiment)	Measured	Calculated (2D)
T	Temperature	Calculated (1D)	Calculated (2D and 3D)
λ_1	CNT-microtip contact resistance	Imposed (1D) (=λ)	Adjusted (2D and 3D)
λ_2	CNT-wall contact resistance	Not considered	Adjusted (2D only)
T_{MAX}	CNT temperature at the breaking point (self-heating experiment)	3400 K (self-heating) 2000 K (field emission)	Self-consistent limit (2D/3D) (1849.5 K)
z_{B}	CNT breaking point location	Measured	Target value for $z_{\text{B(th)}}$
$z_{\text{B(th)}}$	Predicted z_{B} value	Calculated (1D)	Calculated (2D and 3D)

junction with the tungsten microtip were assumed constant and taken from Ref. 18 at a given current I ($k_{\text{CNT}}=100$ W/m.K, thermal contact resistance, $\lambda_1=1.774\times10^7$ K/W). Because the counter-electrode "wall" facing the microtip was massive compared to the rest of the circuit, they assumed the CNT-counter-electrode junction point temperature remained at 300 K. We believe this simplification led to poor estimates for the CNT thermal conductivity and contact resistance. Furthermore, since the applied voltage did not come into play, the 1D model was not consistent with Ohm's law.

We extended the model developed in Ref. 1 to include a thermal contact resistance λ_2 at the contact point of the CNT with the upper wall. Instead of the 1D formulation of the heat equation for a constant current, we used cylindrical coordinates for a CNT exchanging heat through radiation and by conduction at its extremities. Additionally, this 2D model calculates the current I self-consistently from the applied voltage $\Delta\psi$ and resistivity distribution as a function of temperature along the CNT. Table I provides a detailed comparison between the 1D model of Wei *et al.*,[1] the present 2D model dedicated to the CNT self-heating experiment and the 3D model discussed in the next sections of this study.

The results presented in Fig. 3 highlight the discrepancies between the model used in [1] and our 2D model. In this comparative study we used $\lambda_1=1.774\times10^7$ K/W and $k_{\text{CNT}}=100$ W/m.K and then compared the results with $T=300$ K at the wall and with a second contact resistance. Because the heat generated by Joule dissipation escapes mostly through the junctions to the counter-electrode and microtip, a peaked temperature profile is found. The maximum value of the predicted temperature profile, T_{MAX}, defines the predicted distance from the tungsten microtip to the CNT breaking point, $z_{\text{B(Th)}}$. By varying the CNT thermal conductivity, electrical conductivity and thermal contact resistances λ_1 and λ_2 while ensuring a current of 81 μA is reached with an applied voltage of 2.38 V, one can predict more accurately the temperature profile explaining the observed CNT breaking. First, we used the conditions of Wei *et al.*;[1] $k_{\text{CNT}}=100$ W/(m.K), $\lambda_1=1.774\times10^7$ K/W, $\rho_0=8.1395\times10^{-5}$ Ω.m (room temperature value) and $T=300$ K at the wall. For these conditions, our self-consistent model predicts $I=11.5$ μA and $T_{\text{MAX}}<600$ K for 2.38 V (see Fig. 3). In our 2D model we could impose either I or $\Delta\psi$ as a boundary condition and the unspecified parameter was provided consistently with Ohm's law. There is clearly a discrepancy between the predictions resulting from the assumptions of Wei *et al.*[1] and the measurements.

According to Ref. 19 and 20, k_{CNT} values on the order of 100 W/(m.K) are obtained when CNT mats are used to measure k_{CNT}. A similar value has been deduced in Ref. 18 from the data of Purcell *et al.*[21] It is important to note that the

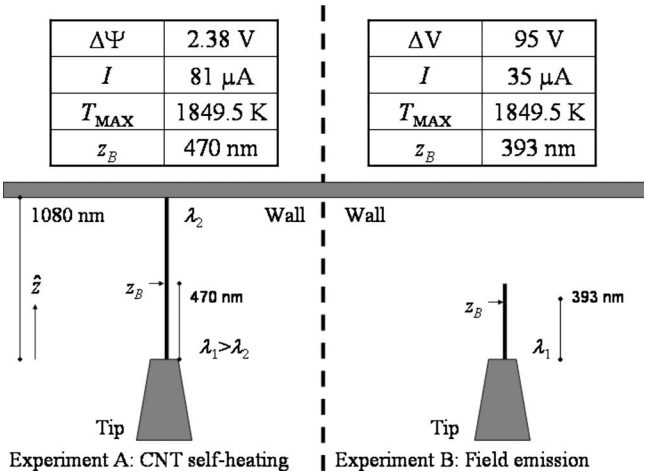

FIG. 2. Schematic of a VACNT mounted on a microtip for the self-heating and field emission experiments.

thermal conductivities deduced from experimental studies are much smaller than the theoretical values, which are at least 10 times larger. If this is indeed the case, the use of CNTs instead of metal nanowires in heat transfer applications becomes questionable. However, according to the comparative study performed in Ref. 19, the low k_{CNT} values are experimental artifacts associated with a poor evaluation of the highly resistive thermal junctions that appear between the CNT and the holding structure. As their results showed, k_{CNT} values as high as 3000 W/(m.K) exist if individual MWCNT are used and a good thermal contact is ensured. On the other hand, when bundles of MWCNT of the same origin are used to measure k_{CNT} (see Ref. 19), the measurements yield lower values. Based on their interpretation and our own calculations, we deduce that the values of $k_{CNT}=100$ W/(m.K) and $\lambda_1=1.774\times10^7$ K/W used in Ref. 1 are both too low to explain the temperature rise and current-voltage values compatible with their experiments.

More heat remains inside the CNT when a more realistic boundary condition is used based on the existence of a thermal contact resistance λ_2 with the wall. Under these circumstances, the position of the CNT breaking point results from the difference between the two contact resistance values rather than from the asymmetry in the boundary conditions imposed in Ref. 1. Because we assume the wall to be a more efficient heat sink than the tungsten microtip, an adjustable parameter $\lambda_1/\lambda_2>1$ was used to shift the location of the peak temperature. We found that λ_1 should be almost doubled with respect to the value used in Ref. 1 in order to trap enough heat into the CNT. Lastly, it appeared that ρ_0 should be set to 3.9×10^{-5} Ω.m for this CNT (referred in Sec. D as Case 1). We cannot explain why the authors' measurements yielded a different result but if we used their estimate of 8.1395×10^{-5} Ω.m we found it was necessary to apply a voltage significantly exceeding 2.38 V for any value of k_{CNT} to reach a current of 81 μA (see Fig. 3). We can point out, however, that since the 8.1395×10^{-5} Ω.m value resulted from an averaging of multiple measurements, the possibility of finding other values on the same order of magnitude was always present. The 3.9×10^{-5} Ω.m value is closer to the generally accepted one used in Ref. 18 and is more consistent with the fact that the CNTs used in Ref. 1 were described as being of high quality.

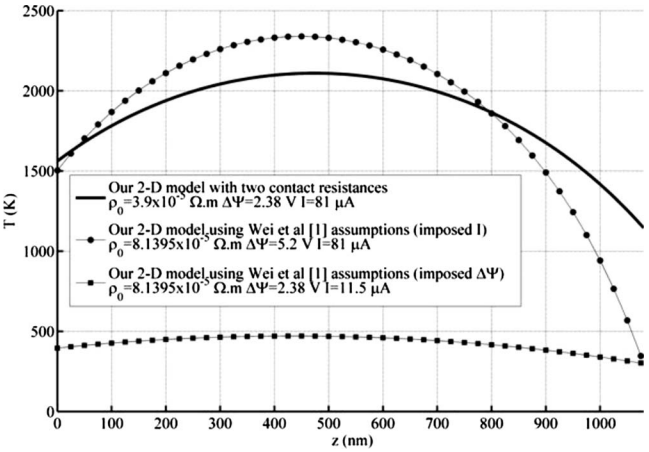

FIG. 3. Comparison between the calculated temperature profiles obtained using the assumptions of Wei *et al.*[1] ($T=300$ K at the wall and either I or $\Delta\psi$ imposed; note Ohm's law is not validated in these cases) and the results we found with a second contact resistance at the wall and the corrected value for ρ_0.

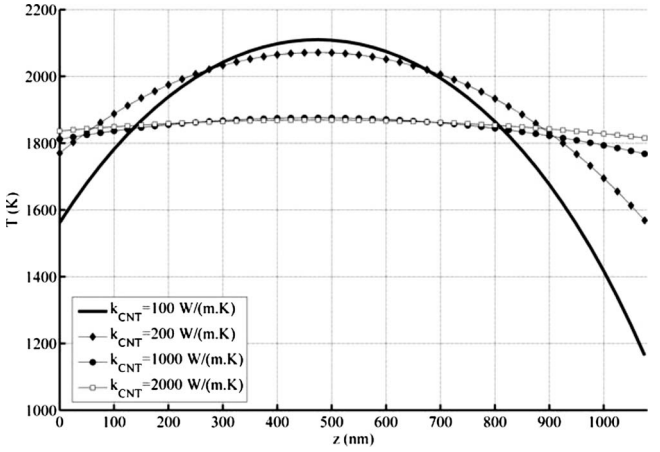

FIG. 4. Temperature profiles along the CNT for Case 1. An increasing value for k_{CNT} reduces T_{MAX} (located at $z=470$ nm) to values within the observed range for temperature-induced CNT breaking. We see that for $k_{CNT}=200$ W/(m.K) and above, the temperature at the CNT tip junction (left) remains almost constant and only T_{MAX} depends significantly of the assumed k_{CNT}. The small total temperature gradients that result are a natural consequence once we accept the measured k_{CNT} reported in Ref. 14.

With our two contact resistances model, we observe that the location of T_{MAX} varies slightly with k_{CNT} for the self-heating experiment and thus, λ_1/λ_2 requires only small adjustments to displace the location of the peak temperature. On the other hand, the actual value of T_{MAX} varies significantly with k_{CNT}. Figure 4 shows, using $k_{CNT}=100$ W/(m.K) and two contact resistances, that a value of $T_{MAX}=2110$ K is found instead of the 3400 K value reported in Ref. 1. For Wei *et al.*,[1] the 3400 K value was problematic because it appeared that $T_{MAX}\sim2000$ K was in fact the limit for field emission according to their 1D model. This result led the authors to suggest that factors other than localized

high temperatures could contribute to the CNT breaking during field emission. Conversely, assuming larger values for k_{CNT} and λ_1 as well as introducing λ_2 actually allow the self-heating and field emission experiments to become consistent in terms of T_{MAX}. Once the value of k_{CNT} reaches 1000 W/(m.K), the value of T_{MAX} stabilizes below 1900 K and for $k_{CNT}=2000$ W/(m.K), we find $T_{MAX}=1849.5$ K. This later value is more consistent with the range of reported values for vacuum experiments (see Ref. 2). At this point, it is worth considering whether impurities or defects could have shifted the location of the breaking point. In the supporting documentation of Ref. 1, the authors report that I initially reached 81 μA and then began to drop down. In this process the CNT walls were destroyed progressively and the CNT became thinner and thinner. If there had been impurities or major defects, the CNT bodies would have appeared bent and angled. In Ref. 17, high resolution images were provided on which individual walls could be counted. The CNT walls were well ordered and evenly spaced, thus suggesting a uniform composition as one could expect from high quality CNT. The smooth shape of the CNT bodies could be verified with the transmission electron microscopy images of Ref. 1 as well.

Another important conclusion of this comparative study is that underestimating simultaneously k_{CNT} and λ_1 can lead to correct predictions of the critical values of I because high temperatures are predicted. However, the longitudinal temperature profile in this case is rather inaccurate. In such profiles, T_{MAX} is too high by a few hundreds of K and the variations of T within the emitter are greatly exaggerated. This particular conclusion also gives a different meaning to predicted acceptable currents when no contact resistance is explicitly assumed, but for which $k_{CNT}=100$ W/(m.K) is used nevertheless. Based on the conclusions drawn in Refs. 19 and 20 and our comparative study, this particular set of assumptions effectively describes a situation where a contact resistance is in fact present and taken into account by assuming a small value of k_{CNT}. Our simple model, combined with suitable estimates for λ_1 and λ_2 and the results of the CNT self-heating experiment can then provide values of k_{CNT} if the oxygen content in the chamber during the experiment imposes a known limit T_{MAX} to the CNT temperature.

From this preliminary study we can identify a suitable set of values for the CNT properties. As we pointed out above, the use of a single value of k_{CNT} defines a unique T_{MAX} value for all samples. In order to compare all samples on the same basis, $k_{CNT}=2000$ W/(m.K) (Ref. 19) and $T_{MAX}=1849.5$ K will be used in every case. The value of λ_1 will be adjusted if necessary (Sec. D) since the quality of the thermal junction varies from one sample to another. As Ref. 18 points out, this parameter can be adjusted to match the experimental conditions. The results presented in Ref. 19 also indicate that the effective contact resistance depends strongly on the geometry of the interface. The $\rho_0=3.9\times10^{-5}$ Ω.m value will be used for Case 1 and as a starting point for other cases. Since statistical fluctuations are possible for this parameter and because no other self-heating experiment was performed prior to field emission measurements with the other samples, the combined effect of given pairs of values for λ_1 and ρ_0 will be discussed for the samples identified as Case 2, Doy_1 and Doy_5.

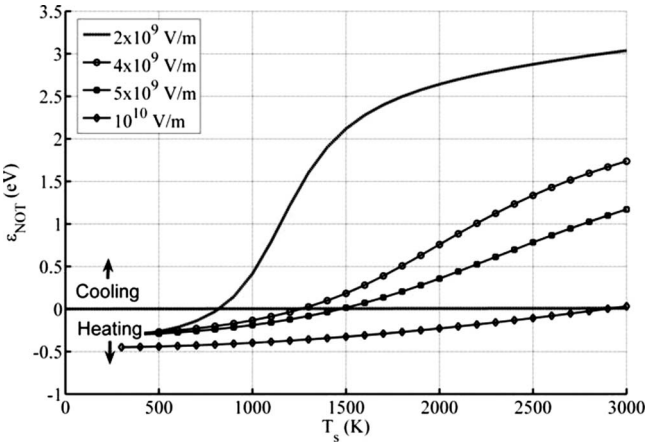

FIG. 5. Nottingham energy exchange ε_{Not} as a function of surface temperature T_s and surface electric field E_s for a work function $\phi_0=4.5$ eV.

B. The Nottingham effect

Figure 5 presents ε_{Not} as calculated using Eqs. (1) and (2) for a range of surface temperatures, T_s, and electric fields, E_s. For a presentation of the evolution of $J_{M\text{-}G}$ for similar ranges of T_s and E_s, the reader is referred to Fig. 1 in Ref. 11. In Ref. 12, these results were provided above 1000 K and as the results of Ref. 11 indicate, large current densities may result from pure field emission at low temperatures for $E_s > 10^9$ V/m. The $\varepsilon_{Not}>0$ area depicted in Fig. 5 indicates that the Nottingham effect acts as a cooling mechanism, whereas for $\varepsilon_{Not}<0$, this process causes heating of the surface. Based on this information, a plausible thermal history associated with a voltage ramp can be suggested. First, a small heating effect may take place. Then, as T_s increases for intermediate E_s values, a cooling effect could occur on the VACNT tip but ultimately, this effect would be lost as $E_s \rightarrow 10^{10}$ V/m because the value of T_{inv} becomes very large.

C. Ideal versus nonideal VACNT array performances

Having estimated the CNT properties using our 2D model with a comparison with experimental results presented in Ref. 1, we then calculated the theoretical performances of CNT arrays placed in good thermal contact with a metal substrate and using k_{CNT} values of 100 and 2000 W/(m.K). These achievable performances are defined as the accessible range of surface-averaged emitted current density J_{eq} (A/m^2). As explained at the end of Sec. A, assuming $k_{CNT}=100$ W/(m.K) limits the heat transfer to the substrate and thus plays a similar role to that of a contact resistance. A value of $k_{CNT}=2000$ W/(m.K) corresponds more closely to the ideal situation. This twentyfold increase in k_{CNT} delays the occurrence of high temperatures and very high J_{eq} values become achievable. Figure 6 shows the $J_{eq}(E_0)$ curves for the first three arrays indicated in Table II assuming $\rho_0=3.9\times10^{-5}$ Ω.m. It can be seen that shorter CNTs, forming

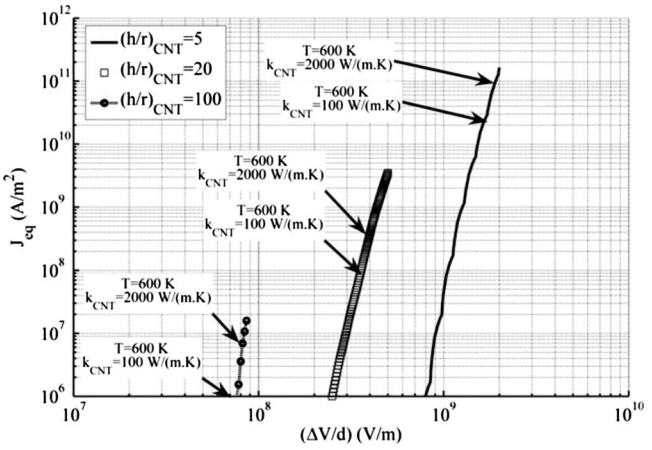

FIG. 6. Equivalent surface-averaged current density J_{eq} as a function of E_0 for three different geometries (ϕ_0=4.5 eV). The arrows indicate at which J_{eq} value the temperature limit of 600 K is reached.

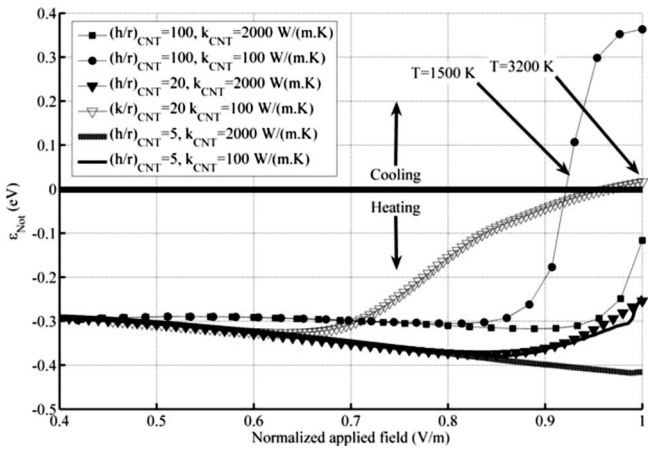

FIG. 7. Nottingham energy exchange ε_{Not} as a function of the normalized applied electric field for three different geometries (ϕ_0 =4.5 eV). A lower k_{CNT} value (nonideal case) hastens the transition to a cooling effect but it takes $(h/r)_{CNT}>20$ to observe it.

denser arrays if $\Delta x=(1\text{-}2)h_{CNT}$, can reach higher surface-averaged current densities. This is due to an increased number of emitters sharing the total current while still being consistent with the definition of the optimal spacing $\Delta x_{optimal}$ minimizing the screening effects, in units of emitter length h.[22] As a consequence, we identified the $(h/r)_{CNT}=5$ case as the most promising geometry for achieving very strong currents. The maximum achievable J_{eq} values depend on the assumptions we make on the acceptable temperature limits and the value of k_{CNT}. We used previous reports[23] on the detrimental effects of oxygen on the CNT structure occurring between 700 and 1000 K to suggest a conservative temperature limit of 600 K. For $(h/r)_{CNT}=100$, 20 and 5, respectively, we find maximum values of 3.4×10^6, 4.45×10^8, and 1.3×10^{11} A/m^2 for $T_S\leq600$ K and $E_s\leq10^{10}$ V/m, assuming $k_{CNT}=2000$ W/(m.K). Because the assumed temperature limit is low, the effect of T_s on $J_{M\text{-}G}$ is negligible.[11] If a vacuum environment is assumed, the temperature-induced CNT destruction process requires that higher temperatures (1500–2000 K) are needed for these destructive effects from trace amounts of oxygen or water to take place.[2] The results from Ref. 24 also indicate that the local current density values inside a current carrying CNT predicted by our model are acceptable.

For the particular study described in Ref. 1 where the high vacuum environment of a transmission electron microscope was used, temperatures around 2000 K were made accessible. Therefore, we allowed the possibility of reaching 3000 K in our calculations to locate the onset of any possible tip cooling effect depending on the assumed thermal properties. We do believe however that for typical experimental conditions much lower temperatures (e.g., 600 K) should be viewed as acceptable to allow reproducible emission currents. Because the M-G theory is valid for $E_s\leq10^{10}$ V/m, we also did not allow this maximum value to be exceeded when assuming large values for E_0. This forced the elimination of some data from Ref. 17 for which we estimated field values $E_s\approx2\times10^{10}$ V/m. With increasing E_0, the value of ε_{Not} travels in the (E_s, T_s) space defined by Fig. 5 as dictated by the effective value of T_s. Figure 7 shows the evolution of ε_{Not} for all three theoretical geometries as a function of the normalized applied electric field. A normalized field is used to facilitate the representation; this normalization uses the values of the applied field varying from one array to another, and divided by the maximal value of E_0 for each ramp. The maximal values can be found in Fig. 6.

TABLE II. Description of the CNT dimensions.

Designation	h_{CNT} (nm)	r_{CNT} (nm)	$(h/r)_{CNT}$
$(h/r)_{CNT}=100$	5000	50	100
$(h/r)_{CNT}=20$	1000	50	20
$(h/r)_{CNT}=5$	100	20	5
Case 1	470	7	67.1
Case 2	330	7	47.1
Doy_1	1000	10.5	95.2
Doy_5	100	2.6	38.4

A key observation can be made from the ε_{Not} curves of Fig. 7: not all arrays experience a significant cooling from the Nottingham effect. This is particularly true if the aspect ratio is low. The presence of a significant contact resistance plays a major role in the occurrence of the tip cooling effect. The Nottingham effect is always present but its influence on the temperature profile is more important if a contact resistance is present or, equivalently, if $k_{CNT}=100$ W/(m.K) is assumed. A larger contact resistance also allows the Nottingham effect to cool the surface at lower fields because T_s increases more rapidly. The array with the longest CNTs show positive ε_{Not} values when T_s is above 1500 K for the $k_{CNT}=100$ W/(m.K) situation. As a consequence, for similar current values the Nottingham effect can be identified as the true source of the peaked T_s profile along the CNT axis when conditions impose $\varepsilon_{Not}\sim0.1$ eV. The $\Delta\varepsilon=1.5k_BT_s$ term used in Ref. 1 to evaluate CNT cooling fails to predict the local heating we now see as the rule rather than the exception for aspect ratios below $(h/r)_{CNT}=20$ with $\phi_0=4.5$ eV. The

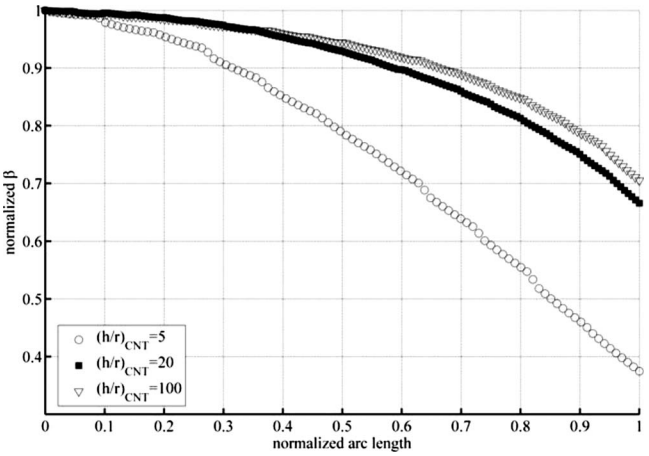

FIG. 8. Normalized β as a function of the normalized distance from the CNT tip for three theoretical geometries. The normalizing factor used is the corresponding maximal β value for each CNT and the total distance $(0.5\pi r_{\mathrm{CNT}})$ between the tip and the edge of the cap.

$(h/r)_{\mathrm{CNT}}=20$ case illustrates very well the limit between the cooling and heating due to the Nottingham effect for the nonideal $k_{\mathrm{CNT}}=100$ W/(m.K) scenario. In the particular case where we assumed $h=1$ μm, only a small peak in the longitudinal temperature profile can be found near the tip, and this only for the range $T_s=3000-3200$ K.

To understand the differences in the evolution of $\varepsilon_{\mathrm{Not}}$ from one geometry to another at a constant k_{CNT}, one must study the spatial profile of β on the CNT cap surface. As $(h/r)_{\mathrm{CNT}}$ decreases, the value of β falls from its maximal value more rapidly when moving away from the CNT axis on the CNT cap (see Fig. 8). As a consequence, the fraction of the tip surface effectively acting as an emitting area decreases for lower values of $(h/r)_{\mathrm{CNT}}$ and becomes more concentrated at the very tip of the VACNT. These differences impose different heat flux distributions that can only be revealed using a 3D model where the β values are computed accurately around the emitters. In other words, only a 3D model properly representing the $\beta(x,y,z,(h/r)_{\mathrm{CNT}},\Delta x)$ structure allows one to observe this effect. One of the consequences of this is that for two different $(h/r)_{\mathrm{CNT}}$ values where r and Δx are kept the same, matching the βE_0 product on the CNT tips of the two arrays by adjusting E_0 does not produce the same J_{eq}. The shorter array requires a small additional increase in E_0 to compensate for the reduction of the emissive area. Thus, for given surface-averaged current density values J_{eq}, the local field E_s at the strongly emissive zone of the tubes needs to be higher for the shorter arrays. Figure 5 indicates that larger E_s are associated with higher T_{inv} values. For $E_s=10^{10}$ V/m, the value of T_{inv} is close to 3000 K. Since the $(h/r)_{\mathrm{CNT}}=5$ array reaches this surface field below 2000 K, it cannot be cooled by Nottingham effect. For $(h/r)_{\mathrm{CNT}}=20$ and $k_{\mathrm{CNT}}=100$ W/(m.K), $\varepsilon_{\mathrm{Not}}$ can only become slightly positive. As a consequence, only very small temperature maxima are observed in the temperature profile and these are located close to the tip.

For $\phi_0=4.5$ eV, one can estimate an aspect ratio of $(h/r)_{\mathrm{CNT}}=20$ to be a good value for a transition criterion between two different destruction mechanisms for the VACNT, especially if a significant contact resistance comes into play. For $(h/r)_{\mathrm{CNT}}$ ratios larger than 20, the presence of peaked longitudinal temperature profiles shifts the maximal temperature away from the emitting tip into the CNT body. As a consequence, once the critical temperature is reached for the etching of carbon from trace amounts of oxygen or water, the emitter eventually breaks at this point. Therefore, whole sections of the CNT are removed and a new cap forms at the tip of the remaining section. If the applied field increases again to create a different temperature profile with a maximum located away from the recently formed tip, a shorter CNT piece is removed. As this process is repeated, the decreasing $(h/r)_{\mathrm{CNT}}$ value will at some point approach the $(h/r)_{\mathrm{CNT}}=20$ limit. The breaking point will eventually be located inside the cap or at the cap boundary with the CNT body (i.e., a distance r from the tip). For lower $(h/r)_{\mathrm{CNT}}$ values, the Nottingham effect only results in a heating of the emitters. The $\Delta\varepsilon=1.5k_BT_s$ assumption made by Wei *et al.*[1] only allows a cooling of the surface, so it would appear that the CNT can withstand even stronger currents. Since $\varepsilon_{\mathrm{Not}}<0$ for these lower $(h/r)_{\mathrm{CNT}}$ values, these emitters are in fact destroyed from their tip and the total heat source is underestimated.

D. Field emission measurements

One can now predict the location of the CNT breaking points for the samples described in Refs. 1 and 17 (see Table II). The experimental conditions we can study include samples identified by Wei *et al.*[1] as Cases 1 and 2 as well as CNT numbers 1 and 5 from Doytcheva *et al.*,[17] which we refer here to Doy_1 and Doy_5. We define the experimentally observed breaking points and associated I-ΔV data as z_{B}, I_{exp}, and ΔV_{exp}. The corresponding breaking point prediction $z_{\mathrm{B(Th)}}$ is provided along with predicted I-ΔV data (I_{th} and ΔV_{th}). We replaced the assumption of a good thermal conduction path between the CNT and the substrate by the empirical expression for the heat loss into a tungsten microtip.[1,18] More energy being trapped into the CNT forces $\varepsilon_{\mathrm{Not}}$ to remain positive at lower applied fields because of the higher temperature. With the introduction of a contact resistance, the overall temperature gradient along the CNT is reduced and the temperature at the CNT base increases significantly. From their I_{exp}-ΔV_{exp} data, Wei *et al.*[1] predicted a maximal temperature T_{MAX} of about 2000 K along the CNT in the region located around the observed breaking point. With our set of properties [larger λ_1, $\rho_0=3.9\times10^{-5}$ Ω.m, and $k_{\mathrm{CNT}}=2000$ W/(m.K)], we recalculated the values of $z_{\mathrm{B(Th)}}$. Larger values of λ_1 and k_{CNT} flatten any temperature profile compared to those predicted with $k_{\mathrm{CNT}}=100$ W/(mK.). Also, because more heat is trapped inside the CNT compared to ideal emitters, the Nottingham effect now almost systematically cools the CNT tips when I_{th} matches the reported I_{exp}. As Fig. 9 shows for $k_{\mathrm{CNT}}=2000$ W/(m.K), an overall gradient of less then 100 K becomes typical and instead of creating a peaked temperature profile, the Nottingham cooling effect produces a relatively narrow isothermal region on the temperature scale. With the

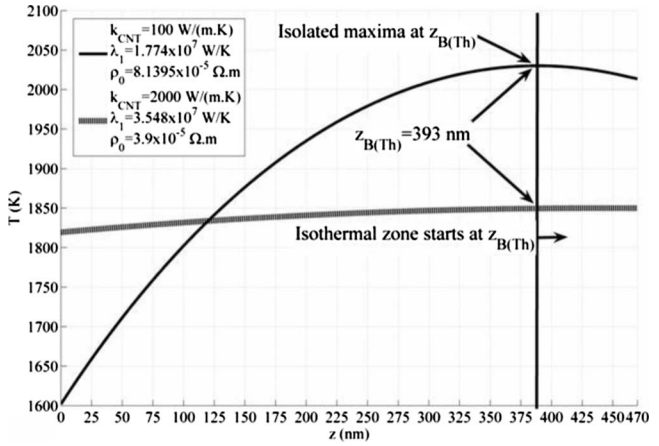

FIG. 9. Temperature profiles along the CNT designated as Case 1 obtained using the CNT properties assumed by Wei *et al.*[1] and our results from Sec. D.1. Both sets of assumption lead to a predicted breaking point at $z=393$ nm but for $k_{CNT}=2000$ W/(m.K), T_{MAX} matches the value we calculated for the self-heating experiment.

corrected set of assumptions, we find that for $\Delta V_{th}=\Delta V_{exp}+/-1$ V and $I_{th}\approx I_{exp}$ (within a few μA), the isothermal zone exceeded $T_{MAX}=1849.5$ K and $z_{B(Th)}=z_B$ marks its beginning (see Table III). For the particular case of Doy_5, this corrected set of properties made the entire length of the CNT uniformly warm and $T_{MAX}=1849.5$ K was exceeded at 250 V for $I=21$ μA.

The CNT dimensions being precisely known, the field enhancement factor can here be calculated accurately. As a consequence, matching the I-ΔV data allows a confirmation of the $\phi_0=4.5$ eV assumption. It is to be noted that the ΔV and ϕ_0 parameters were not used in the 1D model of Wei *et al.* Our ability to match the I-ΔV data with ϕ_0 provides a different method for the evaluation of ϕ_0 from the experimental data available. Inappropriate values of ϕ_0 lead in most cases to very high values of the calculated β parameter in the study of Fowler-Nordheim plots.[11] Calculating consistent values of β, ϕ_0 and T_s at the emission site becomes possible from the I-ΔV data alone using the formulae provided in Ref. 11. According to Bonard *et al.*,[2] $\phi_0=4.5$ eV is an advisable compromise in view of the variations induced by the possible presence of adsorbed water molecules, trace amounts of metal atoms,[25,26] graphitic plane edges or other atoms left on or bonded to the CNT. We found however that small adjustments were effectively necessary. Reducing ϕ_0 has two consequences. First, it allows the current to be stronger at lower voltages. Second, the relevant range of $J_{M\text{-}G}$ values is shifted towards regions of the $(T_s,\ E_s)$ space for which $\varepsilon_{Not}>0$ and more significant surface cooling occurs.

Because the last three samples were not used in self-heating experiments as Case 1, the task of matching the I-ΔV data required changing ρ_0 or λ_1 to fine tune I_{th}. For Case 2, if we used either the same $(\rho_0,\ \lambda_1)$ data as for Case 1 or the data provided in Table III, we found almost identical temperature profiles thus leading to the same $z_{B(Th)}=z_B$. However, with the $(\rho_0,\ \lambda_1)$ data from Case 1 we found $I_{th}=60$ μA while $I_{exp}=40$ μA. Therefore, we see that I_{th} will reasonably match the value of I_{exp} only for a well-adjusted set of ϕ_0, ρ_0, λ_1, $\Delta V_{th}=\Delta V_{exp}$, and k_{CNT} values. With the small emitter used in Case Doy_5, a much more significant fraction (85%) of the total emitter length was affected when the temperature exceeded $T_{MAX}=1849.5$ K. We can see now that the effects of thermal contact resistances and the contribution of the Nottingham effect are responsible for the observed destruction of both long and short emitters. By choosing the proper set of CNT properties and assuming sufficient thermal contact resistances, we also find a consistent temperature limit for both field emission and self-heating experiments.

V. CONCLUSION

We used Murphy and Good theory for thermo-field electron emission, a 2D model for heat conduction and a 3D model for the current transfer to predict the electron emission current from ideal VACNT arrays and the temperature distribution along the CNT axis. The heat transfer model considers the localized Joule heating and Nottingham effect associated with electron emission. Assuming a value of 2000 W/m.K for the CNT thermal conductivity in a simple model for a self-heating experiment including contact resistances for heat transfer, we defined a maximal temperature that is consistent with the calculated temperature profiles for field emission measurements. A different interpretation for the current-induced destruction process of VACNT arrays is proposed based on the evolution of the Nottingham energy exchange providing a heating or a cooling effect during thermo-field emission at high temperatures (1500–3000 K). This mechanism is characterized by a significant cooling of the tips for long, thin $[(h/r)_{CNT}>20]$ emitters that break at their hottest point. With very short emitters, a thermal runaway occurs which process affects at least 85% of the CNT length. This particular result provides an explanation for the unexpected total destruction of short emitters observed by other researchers. High assumed CNT thermal conductivity and inclusion of thermal contact resistances change the shape of the temperature profile compared to the low conductivity and no contact resistance assumptions previously made. In-

TABLE III. Calculated $z_{B(Th)}$ for $k_{CNT}=2000$ W/(m.K) and adjusted values of ϕ_0.

Name in [1, 11]	z_B (nm)	$z_{B(Th)}$ (nm)	ΔV (V)	ΔV_{th} (V)	I_{exp} (μA)	I_{th} (μA)	T_{MAX} (K)	ϕ_0	λ_1 (10^7 W/K)	ρ_0 (10^{-5} Ω.m)
1	390	393	95	94.2816	35	42.6	1849.5	4.3	3.5480	3.9
2	280	280	88	88	40	42.8	1849.5	4.1	2.470738	8.0
Doy_1	900	900	190	190	18	20.7	1849.5	4.9	7.8056	8.0
Doy_5	-	<15	250	250	20	20.6	1849.5	3.05	14.6	3.9

stead of a peaked temperature profile having its highest value at the predicted breaking point, a short isothermal zone was found at the CNT tip. When this zone reaches our calculated critical temperature, it shows the same length as the removed CNT fragments in field emission measurements reported in the literature. Taking into account the 3D geometry of the emitter, our model calculates the effective electric field enhancement for experimental situations and as a result, the emitter work function can be evaluated. Because the predicted surface-averaged emitted current densities are very large, breakdown of the background gas present in the vacuum chamber, and plasma formation above the VACNT arrays can be expected. We will discuss the plasma-VACNT interaction in a forthcoming article.

ACKNOWLEDGMENTS

The authors acknowledge the financial support from the Natural Sciences and Engineering Research Council of Canada (NSERC), the Fonds québécois de la recherche sur la nature et les technologies (FQRNT), and McGill University.

*Corresponding author; martin.dionne@mail.mcgill.ca

[1] W. Wei, Y. Liu, Y. Wei, K. Jiang, L.-M. Peng, and S. Fan, Nano Lett. **7**, 64 (2007).
[2] J.-M. Bonard, H. Kind, T. Stöckli, and L.-O. Nilsson, Solid-State Electron. **45**, 893 (2001).
[3] K. A. Dean, T. P. Burgin, and B. R. Chalamala, Appl. Phys. Lett. **79**, 1873 (2001).
[4] E. L. Murphy and R. H. Good, Phys. Rev. **102**, 1464 (1956).
[5] K. L. Jensen, J. Appl. Phys. **102**, 024911 (2007).
[6] K. L. Jensen, Adv. Imaging Electron Phys. **149**, 274-276 (2007).
[7] R. H. Fowler and L. W. Nordheim, Proc. R. Soc. Lond. A **119**, 173 (1928).
[8] O. W. Richardson, Philos. Trans. R. Soc. **201**, 497 (1903).
[9] S. G. Christov, Phys. Status Solidi **17**, 11 (1966).
[10] S. Coulombe and J.-L. Meunier, J. Phys. D **30**, 776 (1997).
[11] M. Dionne, S. Coulombe, and J.-L. Meunier, J. Phys. D **41**, 245304 (2008).
[12] J. Paulini, T. Klein, and G. Simon, J. Phys. D **26**, 1310 (1993).
[13] G. Fursei, *Field Emission in Vacuum Microelectronics* (Kluwer, New York, 2005).
[14] M. S. Chung, P. H. Cutler, N. M. Miskovsky, and T. E. Sullivan, J. Vac. Sci. Technol. B **12**, 727 (1994).
[15] C. J. Edgcombe and U. Valdrè, J. Microsc. **203**, 188 (2000).
[16] L. Nilsson, O. Groening, C. Emmenegger, O. Kuettel, E. Schaller, and L. Schlapbach, Appl. Phys. Lett. **76**, 2071 (2000).
[17] M. Doytcheva, M. Kaiser, and N. de Jonge, Nanotechnology **17**, 3226 (2006).
[18] N. Y. Huang, J. C. She, J. Chen, S. Z. Deng, N. S. Xu, H. Bishop, S. E. Huq, L. Wang, D. Y. Zhong, E. G. Wang, and D. M. Chen, Phys. Rev. Lett. **93**, 075501 (2004).
[19] P. Kim, L. Shi, A. Majumdar, and P. L. McEuen, Phys. Rev. Lett. **87**, 215502 (2001).
[20] M. Fujii, X. Zhang, H. Xie, H. Ago, K. Takahashi, T. Ikuta, H. Abe, and T. Shimizu, Phys. Rev. Lett. **95**, 065502 (2005).
[21] P. Vincent, S. T. Purcell, C. Journet, and V. T. Binh, Phys. Rev. B **66**, 075406 (2002).
[22] M. Dionne, S. Coulombe, and J.-L. Meunier, IEEE Trans. Electron Devices **55**, 1298 (2008).
[23] R. Brukh and S. Mitra, J. Mater. Chem. **17**, 619 (2007).
[24] P. J. de Pablo, E. Graugnard, B. Walsh, R. P. Andres, S. Datta, and R. Reifenberger, Appl. Phys. Lett. **74**, 323 (1999).
[25] T. Meng, C.-Y. Wang, and S.-Y. Wang, J. Phys.: Condens. Matter **18**, 10521 (2006).
[26] Y.-H. Lee, D. H. Kim, D. H. Kim, and B.-K. Ju, Appl. Phys. Lett. **89**, 083113 (2006).